Magnetization and microwave study of superconducting MgB_2

A. Dulčić, D. Paar, and M. Požek
Department of Physics, Faculty of Science, University of Zagreb, P.O. Box 331, HR-10002 Zagreb, Croatia

G. V. M. Williams
2. Physikalisches Institut, Universität Stuttgart, D-70550 Stuttgart, Germany
and Industrial Research Limited, P.O. Box 31310, Lower Hutt, New Zealand

S. Krämer
2. Physikalisches Institut, Universität Stuttgart, D-70550 Stuttgart, Germany

C. U. Jung, Min-Seok Park, and Sung-Ik Lee
National Creative Research Initiative Center for Superconductivity and Department of Physics,
Pohang University of Science and Technology, Pohang 790-784, Republic of Korea
(Received 17 July 2001; revised manuscript received 25 January 2002; published 21 June 2002)

We report magnetic-field-dependent magnetization and microwave impedance measurements on a MgB_2 superconductor prepared by high-pressure synthesis. We find that the upper critical field is linearly dependent on temperature near T_c and the dc irreversibility field exponent is ~1.4. Microwave surface impedance measurements were carried out in applied magnetic fields up to 8 T. The low-field data show an absence of weak links in the superconducting state. By inverting the surface impedance data, we find a vortex depinning frequency that decreases with increasing magnetic field, which is characteristic of collective pinning.

DOI: 10.1103/PhysRevB.66.014505 PACS number(s): 74.70.Ad, 74.25.Nf, 74.25.Ha

INTRODUCTION

The report of superconductivity in commercially available MgB_2 is proving to be particularly interesting especially as the superconducting transition temperature is relatively high (39 K) for a simple binary structure.[1] Recent Hall effect experiments have shown that the carriers in MgB_2 are holes.[2–4] The observation of a boron isotope effect has led to MgB_2 being described as a phonon-mediated BCS superconductor.[5] Further understanding of superconductivity in MgB_2 is complicated by conflicting reports concerning the magnitude and symmetry of the superconducting gap. Some studies report an *s*-wave superconducting order parameter where $2\Delta/k_BT$ is less than that expected within the weak-coupling BCS theory[6–8] or large enough so that MgB_2 is in the strong-coupling regime.[9] Other studies report the existence of two superconducting gaps[10–13] or nodes in the superconducting gap.[14] It is worth noting that the study of the electronic density of states in MgB_2 has been extended to single crystals.[15] The temperature dependence of the superfluid fraction has been found consistent with a two-gap scenario. Early ^{11}B nuclear magnetic resonance measurements supported the *s*-wave superconducting order parameter model, and a small coherence peak was reported.[9] However, this has been questioned by a later study that accentuated the importance of flux motion to the value of the spin-lattice relaxation rate.[16]

MgB_2 appears to be promising in technological applications. For that purpose tailoring of the physical properties may be achieved by specific sample preparation methods or subsequent treatment.[17] In particular, the achievement of high critical current densities at high magnetic fields would be very attractive, especially in the light of the difficulties with high-temperature superconductors. Among the technologically relevant properties are the temperature dependences of the upper critical field H_{c2} and the magnetic irreversibility field $H_{\rm irr}$. The anisotropy of H_{c2} is very important and has been reported to range from 1.23 to 2.6 (Refs. 18–20) in various samples. Also, some of the reports found that H_{c2} was not linearly dependent on temperature near T_c.[18,19,21–24] It has been suggested that this positive curvature is similar to that observed in the nickel borocarbides and can be explained by a two-band model for superconductivity in the clean limit.[21] However, a linear temperature dependence of H_{c2} was reported in other studies.[20,25,26] The temperature dependence of $H_{\rm irr}$ has also been investigated in various samples.[26–29] Two reports have found that $H_{\rm irr}$ scales linearly with the temperature deviation from T_c,[26,27] while the analysis of $H_{\rm irr}$ reported in two other studies gives a scaling of the form $H_{\rm irr} \propto (T-T_c)^n$, where n is ~1.2 (Ref. 28) or ~1.5 (Ref. 29).

Microwave surface impedance measurements are well suited to investigate fundamental parameters such as the superconducting gap and penetration depth, but also yield information concerning the dissipation which is important in high-frequency applications. Initial measurements of the microwave resistance on separated MgB_2 grains (3 GHz) revealed a relatively high resistance below T_c that could not be explained by a isotropic *s*-wave superconducting order parameter.[30] A similar observation was made from an optical study of MgB_2 thin films with energies ranging from 0.5 to 3.7 meV.[31] Recent microwave studies have concentrated on the low-temperature behavior of the surface resistance $R_s(T)$ and penetration depth $\lambda(T)$ in powder samples and thin films.[32–35] The apparently different temperature dependences in various samples could be interpreted in terms of an anisotropic superconducting gap. In *c*-axis-oriented films the

large superconducting gap $\Delta_{ab} \sim 7.5$ meV is manifested in the microwave properties, whereas in unaligned samples it is the small gap $\Delta_c \sim 3$ meV which determines the electrodynamic response. The impurity phases in various samples yield relatively high residual surface resistance and may influence the detailed shapes of the observed $R_s(T)$ and $\lambda(T)$ curves, particularly at low temperatures where the gap issue is investigated.

The properties of MgB_2 samples prepared at high temperature and high pressure[36] deserve to be thoroughly investigated in view of the potential technological applications. In this paper we report the results from magnetization measurements and microwave surface impedance measurements on a dense MgB_2 sample in dc magnetic fields up to 8 T. Our sample has been characterized previously in a scanning electron microscopy (SEM) study and its dc resistivity and Hall coefficient have also been reported.[3,36,37] We focus on the analysis of H_{c2} and $H_{\rm irr}$ as deduced from magnetization and microwave impedance measurements. We find that collective pinning of vortices at microwave frequencies prevails in hot-pressed MgB_2 samples.

EXPERIMENTAL DETAILS

The MgB_2 sample was prepared by high-pressure (3 GPa) synthesis using commercial MgB_2 powder as described previously.[3,36,37] The sample was sintered at 950 °C and then quenched to room temperature. The density of the sample produced by this preparation method was 2.48 g cm^{-3}. Scanning electron microscopy shows that the grains are well connected and it is not possible to distinguish the boundaries between individual grains within the resolution of the SEM. The sample purity was more than 99% as determined by x-ray diffraction analysis. Its resistivity was $\sim 50\ \mu\Omega$ cm at room temperature and $\sim 20\ \mu\Omega$ cm at 40 K. The superconducting transition width was about 0.4 K for a 10%–90% drop of the resistivity curve. The Hall constant was found to be positive, and the calculated hole carrier density was 1.5×10^{23} cm^{-3} (Ref. 3). A far-infrared study provided evidence that MgB_2 was in the dirty limit.[38]

Magnetization measurements were made using a superconducting quantum interference device (SQUID) magnetometer and applied magnetic fields of up to 60 kG. The ac magnetization measurements were made with an ac magnetic field of 0.05 G and a frequency of 1 kHz. The dc magnetization data show a small ferromagnetic component that is temperature independent for temperatures less than 300 K. This is likely to be due to the Fe impurity clusters in this sample. Similar observations were reported by other researchers.[14,22,39] We estimate the Fe clusters fraction to be no more that 0.02% of the total sample mass from the saturation magnetization of the ferromagnetic impurity.

Microwave measurements at 9.3 GHz were made using the intracavity method. The sample was mounted on a sapphire cold finger and placed in the center of an elliptic ${}_e\mathrm{TE}_{111}$ cavity where the microwave electric field is maximum. The cavity was kept at liquid helium temperature, and the heater and sensor assembly, mounted on the sapphire holder, enabled the sample temperature to be varied. The dc magnetic field was perpendicular to the microwave electric field. The measured quantities were the Q factor and the resonant frequency of the cavity loaded with the sample. The cavity is made of copper with the walls coated with silver and a thin layer of gold in order to protect the walls from oxidation. This results in an unloaded Q factor of 2×10^4, which is lower than the value attainable with superconducting cavities, but offers the advantage that measurements can be made in an applied magnetic field. With the recently introduced modulation technique,[40] we were able to measure the change of the Q factor with a relative precision of 10^{-3}. The resonant frequency was monitored by a microwave counter. The complex frequency shift is given by,[41]

$$\frac{\Delta\tilde{\omega}}{\omega} = \frac{\Delta f}{f} + i\Delta\left(\frac{1}{2Q}\right) = i\alpha\tilde{Z}_s = \alpha(-X_s + iR_s), \qquad (1)$$

where α contains the geometric parameters of the sample and cavity. The complex surface impedance $\tilde{Z}_s = R_s + iX_s$ is related to the complex surface conductivity $\tilde{\sigma}$ by the expression $\tilde{Z}_s = \sqrt{i\mu_0\omega/\tilde{\sigma}}$. The complex frequency shift in Eq. (1) is defined relative to that from an idealized perfect conductor with the same geometry as the actual sample. Since a perfect conductor does not give rise to microwave absorption, we take the empty-cavity Q factor as the reference point from which $\Delta(1/2Q)$ is monitored. Our measurements on hot pressed MgB_2 samples have shown that the slopes of $\Delta f/f$ and $\Delta(1/2Q)$ in the normal state were identical in amplitude, but opposite in sign. This could be taken as evidence that the sample behaved as a normal metal above T_c. In this case, we can determine the offset of $\Delta f/f$, which is experimentally unknown, so that not only the slopes, but also the absolute values satisfy the identity $-\Delta f/f = \Delta(1/2Q)$ in the normal state. This is equivalent to the condition $R_{sn} = X_{sn}$, and therefore $\tilde{\sigma}$ becomes real and is given by σ_n. The absolute values of R_s can be obtained if a calibration measurement is carried out with another sample of the same size but known conductivity so that the geometric factor α in Eq. (1) can be determined. However, the effective surface areas of the two samples are not necessarily equal due to the surface roughness of granular samples. In such cases, it is convenient to normalize all the measured quantities to their values at some temperature in the normal state. The geometric factor α is then eliminated, and the normalized measured quantities are related to the normalized real σ_1/σ_n and imaginary σ_2/σ_n components of the complex conductivity.

RESULTS AND ANALYSIS

It can be seen from ac susceptibility measurements in Fig. 1(a) that the superconducting transition at 38.3 K is very sharp and the superconducting transition width is less than 1 K. This attests to the good quality and connectivity of the hot-pressed MgB_2 sample. It should be noted that measurements on commercial MgB_2 powder samples and ceramic samples sintered at 1 atm can result in broad transitions into the Meissner state.[26,39] The corresponding dc M/H is plotted in Fig. 1(b) for an applied magnetic field of 25 G in both the zero-field-cooled (solid circles) and field-cooled (open

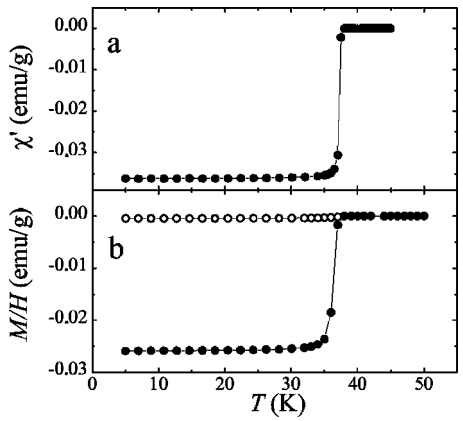

FIG. 1. (a) Plot of the real part of the ac susceptibility against temperature. (b) Plot of the zero-field-cooled (solid circles) and field-cooled (open circles) magnetization divided by the field for an applied magnetic field of 25 G.

circles) conditions. The difference between the zero-field-cooled and field-cooled curves is due to trapped magnetic flux. Note that the remnant magnetic field from the SQUID superconducting magnet is ~6 G, and hence there is some trapped magnetic flux even in the nominally zero-field-cooled condition.

Two important parameters for characterizing type-II superconductors are $H_{\rm irr}$ and H_{c2}. The magnetic irreversibility is apparent in Fig. 2(a) where we show the difference between the field-cooled and zero-field-cooled dc magnetization for different applied magnetic fields. The irreversibility temperature for a given field, $T_{\rm irr}(H)$, is defined by the departure from zero of the corresponding curves plotted in Fig. 2(a). It can be seen that $T_{\rm irr}(H)$ decreases with increasing magnetic field. These data are plotted in Fig. 2(b) as the inverted $H_{\rm irr}(T)$ (open circles). We show by the dashed curve in Fig. 2(b) that $H_{\rm irr}$ can be fitted to $H_{\rm irr}(T)=H_{\rm irr}(0)(1-T/T_c)^n$ over the experimental temperature range where we find that $n=1.4$. The exponent is comparable to that found when a similar function is fitted to the $H_{\rm irr}$ data of Bugoslavsky *et al.* (~1.5),[29] and it is greater than that observed in other MgB_2 samples.[26,28] It is also greater than that reported by Kim *et al.* ($n\sim1.0$),[27] where $H_{\rm irr}$ was defined as the field where the initial negative maximum in the magnetization is observed when the magnetization is measured as a function of increasing magnetic field.

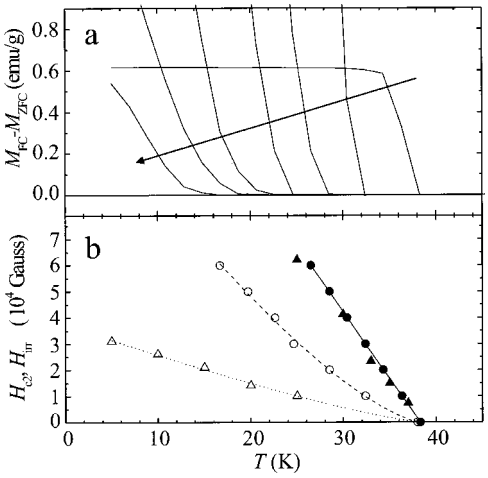

FIG. 2. (a) Plot of the magnetization difference between field-cooled and zero-field-cooled measurements for applied magnetic fields of 60 kG, 50 kG, 40 kG, 30 kG, 20 kG, 10 kG and 25 G. The arrow indicates increasing applied magnetic field. (b) Plot of H_{c2} (solid circles) and $H_{\rm irr}$ (open circles) against temperature. The curves are fits to the data obtained from the magnetization measurements as described in the text. Also shown is H_{c2} (solid triangles) determined from the microwave R_s/R_{sn} using the linear extrapolation method described in the text and the magnetic field where ω_0/ω, plotted in Fig. 6(b) is equal to 1 (open up triangles). The dotted curve is a fit to the microwave data as described in the text.

The origin of the magnetic irreversibility in MgB_2 may include flux-line pinning or flux creep and three-dimensional (3D) flux-lattice melting. We note that the exponent in our MgB_2 sample is close to that obtained from zero-field-cooled and field-cooled magnetization measurements on Nb_3Sn ($n\sim1.37$),[42] where the irreversibility was fitted to the flux-lattice melting model of Houghton, Pelcovitis, and Sudbø.[43] It is therefore possible that the irreversibility in our MgB_2 sample is also due to flux-lattice melting. We show later that the magnetic irreversibility in the microwave region is associated with collective vortex depinning.

It can be seen in Fig. 2(b) that H_{c2} (solid circles) increases linearly with decreasing temperature. H_{c2} was obtained from the temperature-dependent magnetization data where the temperature at which the magnetization begins to decrease in an applied magnetic field defines $H_{c2}(T)$. We find that $dH_{c2}/dT=5100\ {\rm G\,K^{-1}}$ near T_c, which is comparable to that found by Larbalestier *et al.* (~5000 G/K) (Ref. 26) and slightly greater than that found by Finnemore *et al.* (4400 G/K) (Ref. 25). However, other studies have found that $H_{c2}=H^*_{c2}(1-T/T_c)^{1+\alpha}$ where α can be 0.25 or greater.[18,21–23] It has been stated that a positive curvature is also observed in the rare-earth nickel borocarbides, where it has been attributed to an effective two-band model for superconductors in the clean limit.[21] However, as mentioned earlier, a far-infrared study provided evidence that the present MgB_2 samples are in the dirty limit.[38] The presently studied hot-pressed MgB_2 samples belong also to the dirty limit as observed from the relatively high resistivity above T_c. Thus an almost linear $H_{c2}(T)$ is not surprising.

The temperature dependences of R_s/R_{sn} and X_s/X_{sn} are plotted in Fig. 3(a). It can be seen that the transitions into the superconducting state are sharp and there is no evidence of the superconducting fluctuation effects near T_c. At low temperatures the surface resistance shows still relatively high values, which is a sign that impurities play a significant role. This phenomenon has been observed in microwave measurements on other MgB_2 samples.[30,32–35,44,45] The influence of the impurities becomes important if the value of the superconducting gap is determined from the low-temperature penetration depth. In this paper the focus is on the analysis of H_{c2} and $H_{\rm irr}$, which we extract also from field-dependent microwave measurements shown below. However, in order to enable a comparison with other MgB_2 samples measured

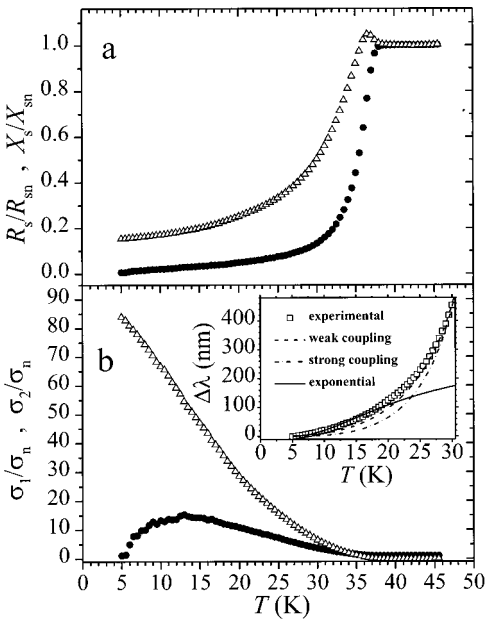

FIG. 3. (a) Plot of R_s/R_{sn} (solid circles) and X_s/X_{sn} (open up triangles) against temperature. (b) The corresponding σ_1/σ_n (solid circles) and σ_2/σ_n (open up triangles) plotted against temperature. The data are normalized to the values at 40 K. The inset shows the temperature variation of the London penetration depth $\Delta\lambda(T)$. The dashed line is the function given by Eq. (3) with $\lambda_0=800$ nm and $n=3\text{-}T/T_c$ for the weak-coupling case, while the dash-dotted line represents the strong-coupling case ($n=4$) with $\lambda_0=1600$ nm. The solid line is exponential behavior given by Eq. (4) with $\Delta/kT_c=1.05$ and $\lambda_0=450$ nm.

in zero-field microwave experiments, we invert the data in Fig. 3(a) to obtain the temperature dependences of the real and imaginary parts of the complex conductivity. In order to deal with the impurities we assume a simple model in which the effective complex conductivity $\tilde{\sigma}_e$ determined by direct inversion of the experimental data is related to the intrinsic complex conductivity $\tilde{\sigma}$ and the impurity contribution by

$$\frac{1}{\tilde{\sigma}_e}=(1-f)\frac{1}{\tilde{\sigma}}+f\rho_i, \tag{2}$$

where f denotes the volume fraction of the impurities and ρ_i their resistivity. Note that Eq. (2) implies the connection in series which is appropriate when the impurities are dispersed on the scale of the microwave penetration depth. The direct inversion of the data in Fig. 3(a) yields $\tilde{\sigma}_e$, and $\tilde{\sigma}$ can be found from Eq. (2) with the choice of f which minimizes the real part σ_1 at low temperatures. Figures 3(b) shows the resulting temperature dependences of $\sigma_1(T)$ and $\sigma_2(T)$. It was calculated assuming ρ_i is equal to the normal-state resistivity ρ_n and $f=0.08$, but no significant change is obtained with $\rho_i>\rho_n$ and corresponding recalculation of f. We note that the obtained values of f are consistent with the estimated volume fractions of Fe impurity clusters as mentioned above. However, other impurities such as Mg and related oxides are not excluded. The resulting complex conductivity in Fig. 3(b) can be compared to the recent microwave measurements on other MgB_2 samples[32–35] through the analysis of the penetration depth $\lambda=(\mu_0\omega\sigma_2)^{-1/2}$ shown in the inset to Fig. 3(b). We plot also the analytical function[32,33]

$$\Delta\lambda(T)=\lambda(T)-\lambda(0)=\lambda_0\left[\frac{1}{\sqrt{1-\left(\frac{T}{T_c}\right)^n}}-1\right], \tag{3}$$

which approximates the temperature variation for strong coupling ($n=4$) and weak coupling ($n=3-T/T_c$) at higher temperatures. It appears that our data fit better to the weak coupling as expected in unaligned samples.[32] For $T\ll T_c$ the temperature dependence is better approximated by an exponential[33]

$$\Delta\lambda\approx\lambda_0\sqrt{\frac{\pi}{2}\frac{\Delta}{kT_c}\frac{T_c}{T}}\exp\left(-\frac{\Delta}{kT_c}\frac{T_c}{T}\right). \tag{4}$$

The solid line in the inset to Fig. 3(b) is the best fit to the experimental low-temperature data obtained with $(\Delta/kT_c)=1.05$. This value is in a good agreement with the values found by other authors.[32–34]

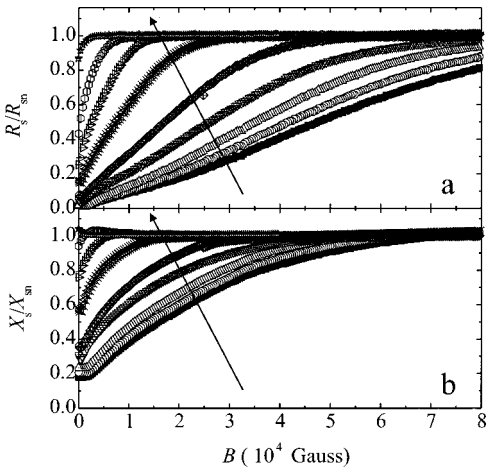

FIG. 4. (a) Plot of R_s/R_{sn} against magnetic field for temperatures of 5, 10, 15, 20, 25, 30, 33, 35, and 37 K. (b) Plot of X_s/X_{sn} against magnetic field for the same temperatures. The arrows indicate increasing temperature.

We now turn to the main objective of the present paper which is the analysis of H_{c2} and $H_{\rm irr}$. These parameters can be determined from the field-dependent microwave measurements. One may note that higher fields are equivalent to higher temperatures where the contribution of impurities is less critical for a proper analysis. Hence our conclusions on H_{c2} and $H_{\rm irr}$ are much less sensitive to possible variations in the treatment of the impurities.

In Fig. 4 we plot R_s/R_{sn} and X_s/X_{sn} against the magnetic field and at different temperatures. It is clear that there are no weak links in our sample because weak links are known to cause a rapid initial increase in R_s and X_s especially in the sintered ceramic high-temperature superconducting (HTSC) samples,[46–48] which is not seen in Fig. 4. The same property has been reported for higher-quality *c*-axis-oriented MgB_2 films.[34] The absence of weak links indicates very good connectivity of the grains in our hot-pressed sample. It also

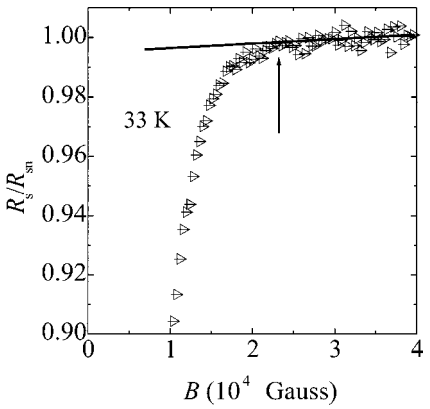

FIG. 5. Plot of R_s/R_{sn} against magnetic field at 33 K on an expanded scale. The arrow indicates the field where R_s/R_{sn} starts to deviate from a straight line, which is taken as H_{c2}.

shows the technological potential of MgB_2 when compared with the HTSC's because the electronic and magnetic properties of the main HTSC being developed for wire application, $Bi_2Sr_2Ca_2Cu_3O_{10+\delta}$, are significantly affected by weak links.

We estimate H_{c2} from the curves in Fig. 4 by performing a linear extrapolation above T_c. This procedure is clear in Fig. 5 where we plot R_s/R_{sn} at 33 K. The departure from the straight line, indicated by the arrow, is the temperature where H_{c2} is equal to the applied magnetic field. The results obtained at various temperatures are summarized in Fig. 2(b) (solid up triangles). It is apparent that this method of determining H_{c2} yields similar results as the method based on the magnetization data.

It is also possible to estimate H_{c2} from the R_s and X_s data plotted in Fig. 4 by considering the effective conductivity $\tilde{\sigma}_H$ in the mixed state which can be expressed as[49]

$$\frac{1}{\tilde{\sigma}_H}=\frac{1-(H/H_{c2})(1-i\omega_0/\omega)^{-1}}{(1-H/H_{c2})(\sigma_1-i\sigma_2)+\sigma_n H/H_{c2}} + \frac{H}{H_{c2}\sigma_n}\frac{1}{1-i\omega_0/\omega}, \tag{5}$$

where ω is the microwave angular frequency and ω_0 is the depinning angular frequency. It can be seen that $\tilde{\sigma}_H$ reduces to the zero-field conductivity, $\sigma_1-i\sigma_2$, when H is zero. Furthermore, as $H\rightarrow H_{c2}$ the effective conductivity tends towards the normal-state conductivity σ_n. In the analysis of the field-dependent measurements, $\tilde{\sigma}_H$ replaces $\tilde{\sigma}$ in Eq. (2). The ratio H/H_{c2} defines the volume fraction of the sample filled by the vortex cores. The concept of an effective conductivity is valid when the distance between vortices is much smaller than the penetration depth. Hence it is not applicable at low magnetic fields. This model assumes that the radius of the vortex cores is $\xi=\sqrt{\Phi_0/2\pi H_{c2}}$, where Φ_0 is the flux quantum. At a constant temperature, the density of vortices increases with increasing magnetic field, but all the vortices have the same fixed radius ξ. Thus H_{c2} in Eq. (5) is defined as a parameter which determines the radius of the vortices at all magnetic fields in the mixed state. The depinning angular

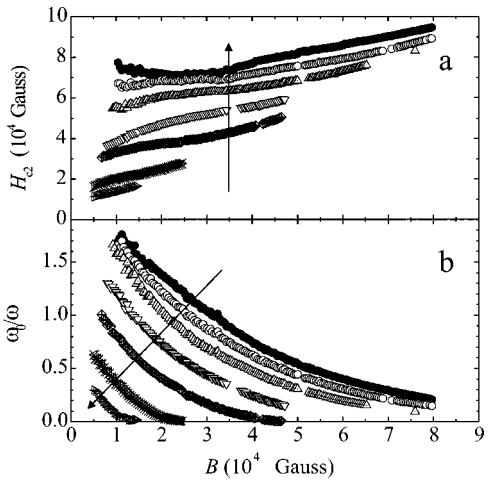

FIG. 6. Plot of H_{c2} and ω_0/ω obtained by numerically inverting of the data from Fig. 5 as described in the text. The arrows indicate increasing temperatures from 5 to 33 K.

frequency parameter ω_0 depends on the pinning potential experienced by the vortices driven by the oscillating microwave current.[50]

We plot, in Fig. 6, H_{c2} and ω_0/ω against applied magnetic field where H_{c2} and ω_0/ω were obtained using Eq. (5), the data in Fig. 4, and the zero-field values of σ_1/σ_n and σ_2/σ_n plotted in Fig. 3(b). We first discuss the depinning frequency. The absolute value of the depinning frequency can be calculated from the data in Fig. 6 and the knowledge of our operating frequency $\omega/2\pi=9.3$ GHz. At low temperatures and low fields the depinning frequency is very high as is the case also in high-temperature superconductors.[50] In general, at a fixed temperature, ω_0 decreases with increasing applied magnetic field, thus showing that the pinning potential is reduced as the density increases. This observation indicates that collective pinning of vortices occurs over the whole magnetic field region covered in Fig. 6. In contrast, a field-independent ω_0 is observed in HTSC's at fields much lower than H_{c2}, which is due to individual vortex pinning.[50] When the pinning is individual the pinning potential depends only on temperature and ω_0 is independent of magnetic field at a given temperature. In collective pinning, however, the effective pinning potential depends on the interactions between vortices and this brings about the field dependence of ω_0. We note that the vortex solid occurs in the irreversible region where $\omega_0/\omega\gg 1$, while for $\omega_0/\omega<1$ there is a gradual transition into the reversible region with decreasing ω_0/ω. The flux-flow regime occurs when $\omega_0/\omega\ll 1$. Therefore, the data in Fig. 6(b) indicate that the magnetic irreversibility observed in the microwave region is associated with vortex depinning. However, the irreversibility field obtained in the microwave region is less than that observed in the dc case. This can be seen in Fig. 2(b) where we plot the magnetic field where $\omega_0/\omega=1$. This is expected since depinning at microwave frequencies is a collective excitation of the flux line lattice, but with flux still trapped in the sample. Depinning in the context of dc magnetization means that the flux has to move across the sample surface. We expect that these different processes appear at different energies. For the dc

magnetization case, depinning is thermally activated and only controlled by the temperature. In the microwave case, depinning is manifested when the viscous drag force, which is proportional to the velocity of the oscillating flux lines, becomes comparable to the restoring force due to pinning in a potential well. This occurs at a temperature lower than that required for the dc magnetization depinning. We show by the dotted curves in Fig. 2(b) that the magnetic field where $\omega_0/\omega=1$ is proportional to $(1-T/T_c)^n$ where $n=1.25$. This line represents the dynamic irreversibility at 9.3 GHz.

It is apparent in Fig. 6(a) that H_{c2}, calculated using the mixed-state model discussed above, is more complex than those plotted in Fig. 2(b). In particular, the inversion process reveals H_{c2} values that increase with increasing applied magnetic field. In a single-crystal superconductor one should get a single constant value for H_{c2} since it reflects the value of ξ, which is constant at a given temperature. We attribute the increase in H_{c2} with increasing field to an intrinsic anisotropy in H_{c2} and random orientations of the grains. When the applied magnetic field is increased above the lowest value of the anisotropic H_{c2}, some of the grains are brought to the normal state and only those grains with orientations yielding higher H_{c2} remain superconducting. In this way, the increasing applied magnetic field gradually changes the average H_{c2} of the grains that still remain in the superconducting state. We note that Eq. (5) is highly nonlinear and the value of H_{c2}, calculated by the inversion procedure from the experimental data, is not a simple average of the intrinsic H_{c2} from the individual grains. The result in Fig. 6 merely proves that there is no single value for H_{c2} at a given temperature, which indicates that the sample has randomly oriented grains with an intrinsic anisotropy in H_{c2}. We note that the value of H_{c2}, obtained from the dc magnetization data and the temperature where the microwave resistance begins to decrease, is the magnetic field where the last grains in the sample are brought into the normal state. Thus, for an anisotropic and unoriented superconductor, this method will provide H_{c2} values that are close to the highest intrinsic upper critical field, which is the one obtained for the magnetic field applied along the *c* axis. In addition, the superconducting fluctuations at the transition from superconducting to normal state at high magnetic fields may produce a curvature in R_s/R_{sn} such as seen for example in Fig. 5 so that the values of H_{c2} defined by the criterion of deviation of R_s/R_{sn} from a straight line turn out to be higher.

CONCLUSION

In conclusion, we have performed magnetization and microwave measurements on dense hot-pressed MgB_2. The magnetic-field-dependent microwave impedance shows no evidence of Josephson weak links, which indicates that the crystal defects and intergranular regions are significantly smaller that the superconducting coherence length. Furthermore, we find that the upper critical field is linearly dependent on temperature and the dc irreversibility field coefficient is larger than that found in some of the previous studies. We show from our analysis of the microwave data that the vortex pinning is collective, which is different from that observed in the HTSC's where individual vortex pinning is observed. Furthermore, the magnetic irreversibility in the microwave region is due to dynamic vortex depinning.

ACKNOWLEDGMENTS

We acknowledge funding support from the Croatian Ministry of Science and Technology (A.D., D.P., and M.P.), the New Zealand Marsden Fund (G.V.M.W.), the Alexander von Humboldt Foundation (G.V.M.W.), and the Ministry of Science and Technology of Korea through the Creative Research Initiative Program (C.U.J, M.-S.P., and S.-I.L.).

[1] J. Nagamatsu, N. Nakagawa, T. Muranaka, Y. Zenitani, and J. Akimitsu, Nature (London) **410**, 63 (2001).
[2] W. N. Kang, Hyeong-Jin Kim, Eun-Mi Choi, Kijoon H. P. Kim, and Sung-Ik Lee, Science **292**, 1521 (2001).
[3] W. N. Kang, C. U. Jung, Kijoon H. P. Kim, Min-Seok Park, S. Y. Lee, Hyeong-Jin Kim, Eun-Mi Choi, Kyung Hee Kim, Mun-Seog Kim, and Sung-Ik Lee, Appl. Phys. Lett. **78**, 4157 (2001).
[4] W. N. Kang, Hyeong-Jin Kim, Eun-Mi Choi, Kijoon H. P. Kim, and Sung-Ik Lee, Phys. Rev. B **65**, 134508 (2002).
[5] S. L. Bud'ko, G. Lapertot, C. Petrovic, C. E. Cunningham, N. Anderson, and P. C. Canfield, Phys. Rev. Lett. **86**, 1877 (2001).
[6] T. Takahashi, T. Sato, S. Souma, T. Muranaka, and J. Akimitsu, Phys. Rev. Lett. **86**, 4915 (2001).
[7] R. A. Kaindl, M. A. Carnahan, J. Orenstein, D. S. Chemla, H. M. Christen, H.-Y. Zhai, M. Paranthaman, and D. H. Lowndes, Phys. Rev. Lett. **88**, 027003 (2002).
[8] G. Karapetrov, M. Iavarone, W. L. Kwok, G. W. Crabtree, and D. G. Hinks, Phys. Rev. Lett. **86**, 4374 (2001).
[9] H. Kotegawa, K. Ishida, Y. Kitaoka, T. Muranaka, and J. Akimitsu, Phys. Rev. Lett. **86**, 5767 (2001).
[10] S. Tsuda, T. Yokoya, T. Kiss, Y. Takano, K. Togano, H. Kitou, H. Ihara, and S. Shin, cond-mat/0104489 (unpublished).
[11] F. Giubileo, D. Roditchev, W. Sacks, R. Lamy, and J. Klein, cond-mat/0105146 (unpublished).
[12] F. Bouquet, R. A. Fisher, N. E. Phillips, D. G. Hinks, and J. D. Jorgensen, Phys. Rev. Lett. **87**, 047001 (2001).
[13] C.-T. Chen, P. Seneor, N.-C. Yeh, R. P. Yasquez, C. U. Jung, and Min-Seok Park, Phys. Rev. B **65**, 012505 (2002).
[14] C. Panagopoulos, B. D. Rainford, T. Xiang, C. A. Scott, M. Kambara, and I. H. Inoue, Phys. Rev. B **64**, 094514 (2001).
[15] F. Manzano, A. Carrington, N. E. Hussey, S. Lee, A. Yamamoto, and S. Tajima, Phys. Rev. Lett. **88**, 047002 (2002).
[16] J. K. Jung, S. H. Baek, F. Borsa, S. L. Bud'ko, G. Lapertot, and P. C. Canfield, Phys. Rev. B **64**, 012514 (2001).
[17] Y. Bugoslavski *et al.*, Nature (London) **411**, 561 (2001).
[18] O. F. de Lima, C. A. Cardoso, R. A. Ribeiro, M. A. Avila, and A. A. Coelho, Phys. Rev. Lett. **86**, 5974 (2001).
[19] M. Xu, H. Kitazawa, Y. Takano, J. Ye, K. Nishida, H. Abe, A.

Matsushita, and G. Kido, Appl. Phys. Lett. **79**, 2779 (2001).
[20] M. H. Jung, M. Jaime, A. H. Lacerda, C. S. Boebinger, W. N. Kang, H. J. Kim, E. M. Choi, and S. I. Lee, Chem. Phys. Lett. **343**, 447 (2001).
[21] K. H. Müller, G. Fuchs, A. Handstein, K. Nenkov, V. N. Narozhnyi, and D. Eckert, J. Alloys Compd. **322**, L10 (2001).
[22] A. G. Joshi, C. G. S. Pillai, P. Rai, and S. K. Malik, Solid State Commun. **118**, 445 (2001).
[23] Y. Takano, H. Takeya, H. Fuji, H. Kumakura, T. Hatano, K. Togano, H. Kito, and H. Ihara, Appl. Phys. Lett. **78**, 2914 (2001).
[24] C. Ferdeghini *et al.*, cond-mat/0109536 (unpublished).
[25] D. Finnemore, J. E. Ostenson, S. L. Bud'ko, G. Lapertot, and P. C. Cranfield, Phys. Rev. Lett. **86**, 2420 (2001).
[26] D. C. Larbalestier *et al.*, Nature (London) **410**, 343 (2001).
[27] Mun-Seog Kim, C. U. Jung, Min-Seok Park, S. Y. Lee, Kijoon H. P. Kim, W. N. Kang, and Sung-Ik Lee, Phys. Rev. B **64**, 012511 (2001).
[28] G. Fuchs, K.-H. Müller, A. Handstein, K. Nenkov, V. N. Narozhnyi, D. Eckert, M. Wolf, and L. Schultz, Solid State Commun. **118**, 497 (2001).
[29] Y. Bugoslavski, G. K. Perkins, X. Qi, L. F. Cohen, and A. D. Caplin, Nature (London) **410**, 563 (2001).
[30] A. A. Zhukov *et al.*, cond-mat/0103587 (unpublished).
[31] A. V. Pronin, A. Pimenov, A. Loidl, and S. I. Krasnosvobodtsev, Phys. Rev. Lett. **87**, 097003 (2001).
[32] A. A. Zhukov *et al.*, cond-mat/0107240 (unpublished).
[33] N. Klein *et al.*, cond-mat/0107259 (unpublished).
[34] A. A. Zhukov *et al.*, cond-mat/0109397 (unpublished).
[35] A. Andreone *et al.*, cond-mat/0109465 (unpublished).
[36] C. U. Jung, Min-Seok Park, W. N. Kang, S. Y. Lee, and Sung-Ik Lee, Physica C **353**, 162 (2001).
[37] C. U. Jung, Min-Seok Park, W. N. Kang, Mun-Seog Kim, Kijoon H. P. Kim, S. Y. Lee, and Sung-Ik Lee, Appl. Phys. Lett. **78**, 4157 (2001).
[38] J. H. Jung, K. W. Kim, H. J. Lee, M. W. Kim, T. W. Noh, W. N. Kang, Hyeong-Jin Kim, Eun-Mi Choi, C. U. Jung, and Sung-Ik Lee, Phys. Rev. B **65**, 052413 (2002).
[39] Y. Wang, T. Plackowski, and A. Junod, Physica C **355**, 179 (2001).
[40] B. Nebendahal, D.-N. Peligrad, M. Požek, A. Dulčić, and M. Mehring, Rev. Sci. Instrum. **72**, 1876 (2001).
[41] D. N. Peligrad, B. Nebendahl, C. Kessler, M. Mehring, A. Dulčić, M. Požek, and D. Paar, Phys. Rev. B **58**, 11 652 (1998).
[42] M. Suenaga, A. K. Ghosh, Y. Xu, and D. O. Welch, Phys. Rev. Lett. **66**, 1777 (1991).
[43] A. Houghton, R. A. Pelcovitis, and S. Sudbø, Phys. Rev. B **40**, 6763 (1989).
[44] N. Hakim, P. V. Parimi, C. Kusko, S. Sridhar, P. C. Canfield, S. L. Bud'ko, and D. K. Finnemore, Appl. Phys. Lett. **78**, 4160 (2001).
[45] Sang Young Lee, J. H. Lee, Jung Hun Lee, J. S. Ryu, J. Lim, S. M. Moon, H. N. Lee, H. G. Kim, and B. Oh, Appl. Phys. Lett. **79**, 3299 (2001).
[46] M. Požek, A. Dulčić, and B. Rakvin, Physica C **197**, 175 (1992).
[47] *Microwave Studies of High Temperature Superconductors*, Vols. 17 and 18 of *Studies of High Temperature Superconductors*, edited by A. Narlikar (Nova Science, Commack, NY, 1996).
[48] M. Požek, A. Dulčić, D. Paar, G. V. M. Williams, and S. Krämer, Phys. Rev. B **64**, 064508 (2001).
[49] A. Dulčić and M. Požek, Physica C **218**, 449 (1993).
[50] M. Golosowsky, M. Tsindlekht, and D. Davidov, Supercond. Sci. Technol. **9**, 1 (1996).